

Population statistics of beamed sources. I

I. Liodakis^{1*} and V. Pavlidou^{1,2}

¹*Department of Physics and ITCP†, University of Crete, 71003, Heraklion, Greece*

²*Foundation for Research and Technology - Hellas, IESL, Voutes, 7110 Heraklion, Greece*

16 June 2015

ABSTRACT

Observations of blazar jets are shrouded in relativistic effects, thus hindering our understanding of their intrinsic properties and dominant physical processes responsible for their generation, evolution, radiation and particle emission. In this work we focus on extracting information about timescales in the jet rest frame using a population-modeling approach. We employ Monte Carlo simulations to derive a simple population model for the intrinsic unbeamed luminosities and the Lorentz Γ of blazar jets that adequately describe the observed redshift and apparent superluminal speed distributions for flux-limited blazar samples. We derive separate models for BL Lacs and Flat Spectrum Radio Quasars. We then use these models to compute the predicted distribution of Doppler factors in each blazar class, and address the following questions: (a) What is the relativistically induced spread in observed timescales (e.g., event duration, time lags) in a flux-limited sample of relativistic jets? (b) Could differences between BL Lacs and FSRQs observed in the time domain be attributed to differences in beaming between the two populations? (c) Is there a statistically preferred amount of beaming in a flux-limited sample? How large are statistical deviations from that preferred value? We use our findings to propose promising approaches in phenomenological studies of timescales in blazar jets.

Key words: galaxies: active – galaxies: jets

1 INTRODUCTION

Blazars are active galactic nuclei (AGN) with jets oriented within a small angle from our line of sight (Blandford & Königl 1979). Because of their preferential alignment, their observed properties are obscured by relativistic effects such as Doppler boosting of their emission, compression of variability timescales, and apparently superluminal motions of resolved jet components. Small variations in the degree of alignment with the line of sight can result to a large scatter in the resulting observable quantities from otherwise similar sources. These effects complicate our understanding of their intrinsic properties and the processes relevant to their central engines.

Blazars are extremely variable broadband emitters. Despite decades of systematic study of their variability properties across the electromagnetic spectrum, little is known regarding the variability properties of blazars as a population *in the jet rest frame*, because of the difficulties involved in directly measuring the Doppler factor of blazar jets. One

approach that has been used to that end is to identify the shortest-duration flare that has been observed in an object, and compare it with some known rest-frame timescale one can associate with the source (for example the light-crossing time of the central black hole, see e.g. Aharonian et al. (2007); or, in radio wavelengths, the size of an emission region of known brightness temperature such as the equipartition, e.g. Readhead 1994; Lähteenmäki & Valtaoja 1999; Hovatta et al. 2009.) These approaches are valuable since they constitute our only way to assess Doppler boosting on a source-by-source basis. However, these methods have well-known drawbacks. First of all, the shortest observed timescale only gives a limit to the observed Doppler factor even if all other assumptions hold exactly, as blazar lightcurves have power-law power spectra (Abdo et al. 2010; Chatterjee et al. 2008). Second, the use of other known physical parameters of the jet, such as the black hole mass, to derive Doppler factors, prohibits any correlation studies between these parameters and Doppler factors.

Although these difficulties cannot be easily circumvented on a blazar-by-blazar basis, the connection between observed and intrinsic (jet rest frame) variability properties for blazars *as a population* can be assessed in a more straight-forward way. Assuming randomly distributed line-

* liodakis@physics.uoc.gr

† Institute for Theoretical and Computational Physics, formerly Institute for Plasma Physics

of-sight orientations for active galactic nuclei jets, we can seek the distribution of intrinsic jet parameters (rest-frame luminosities and Lorentz factors) that best reproduce well-defined observables (such as redshifts and apparent superluminal speeds) rather than the Doppler factors themselves. Then, from these distributions, we can calculate the Doppler factor distribution for the blazar population. We can then use this distribution to deconvolve the Doppler-factor effects on the population as a whole, and gain a statistical insight on the rest-frame variability properties. In this way, we can address questions such as:

- (a) What is the relativistically induced spread in observed event timescales? Could blazar behaviors in the time domain observed to be very varied be in fact very similar in the jet rest frame?
- (b) How different is the beaming between sources in flux-limited samples? Lacking any additional information, is it useful to make statistics-based assumptions for the viewing angle of a single source?
- (c) Do BL Lacs and Flat Spectrum Radio Quasars (FSRQs) have different beaming properties? Could differences observed between them in the time domain be attributed to how relativistic effects differently affect each population?

Our primary motivations for this work are: (i) the study of blazar events of a well-defined duration, such as swings of the polarization angle seen in the optopolarimetric study of blazars (especially in light of currently ongoing large-sample, high-cadence optopolarimetric monitoring programmes such as RoboPol, Pavlidou et al. 2014); and (ii) the study of time lags between different types of events (e.g., between flares at different wavelengths, or between polarization angle swings and flares). However our results are general and can be applied to any time-domain studies of blazar jets.

This paper is organized as follows. In §2 we describe our model for the blazar population. In §3 we discuss the sample we use in order to derive model parameters. In §4 we present our optimization procedure: our model acceptability criteria, the set of observables we have required our model to reproduce, and our optimization algorithm. In §5 we present our results for our samples and in §6 and §7 we discuss the validity of our model and computations, their implementation and the conclusions derived from this work.

The cosmology we have adopted throughout this work is $H_0 = 71 \text{ km s}^{-1} \text{ Mpc}^{-1}$, $\Omega_m = 0.27$ and $\Omega_\Lambda = 1 - \Omega_m$ (Komatsu et al. 2009). This choice was made so that our cosmological parameters agree with the MOJAVE (Monitoring Of Jets in Active galactic nuclei with VLBA Experiment, Lister & Homan 2005) analysis (Lister et al. 2009b).

2 MODEL

The purpose of our model is to simulate observations from a flux-limited sample of blazars. The population model will consist of a joint distribution for the intrinsic, unbeamed luminosity at a specific (radio) wavelength at different redshifts, and for the jet Lorentz factor. From these, assuming a uniform distribution of viewing angles *for the population*, we can then calculate our observables: flux density as measured by the observer, and redshifts and apparent superluminal speeds for sources above a certain flux limit.

Once we identify model parameters for which the distribution of observables are adequately reproduced for a well-defined sample, we can then calculate the distribution of hard-to-observe quantities *for the sample*, such as viewing angles and Doppler factors.

The idea of building a population model for beamed sources is not new. Models have been fitted by, e.g. Padovani & Urry (1992); Padovani (1992); Vermeulen & Cohen (1994); Lister & Marscher (1997). More recently, the observation of jet speeds by the MOJAVE program for a large, flux-limited sample of blazars, the large majority of which have measured redshifts, has provided an unprecedented set of observables against which such models can be tested and re-optimized (see, e.g., Cara & Lister 2008b).

Here, we optimize a new population model for the blazar population. The reasons why this was necessary in order to address the specific issues we are after, and the associated ways our model differs from past work using the MOJAVE dataset are summarized below.

- *We treat BL Lacs and FSRQs as distinct populations.* As the interpretation of optical wavelength data is one of our primary motivations, deriving (potentially) different models for optically distinct classes of blazars (Giommi et al. 2012) is important in order to assess any differences between these classes in the time domain.
- *We do not seek to reproduce the normalization of the luminosity function.* As our luminosity function model is that of pure luminosity evolution (up to a maximum redshift), this implies that the total number density of sources remains constant, and the total number of sources in a redshift interval is simply proportional to the volume element in that same interval. Our purpose is to determine the distribution of these sources among different (unbeamed) luminosity values rather than the total number of sources in any interval. For this reason, we have the flexibility to simply remove from our sample any sources with unknown redshift. This choice does not affect our luminosity distribution under one of the following two assumptions: if *either* the sources without a redshift measurement have the same redshift distribution as the sources with measured redshifts; *or* all of the sources without a redshift measurement reside at higher redshifts than the sources with measured redshifts, due to a bias in our ability to measure redshifts favoring nearby sources. In the latter case, we will incorrectly surmise that the luminosity distribution sharply cuts off above a redshift that is too low, but the luminosity distribution at redshifts where we can measure it will be in general correct.
- *We do not include individual blazar flux densities in the set of observables the distributions of which our model has to reproduce.* The reason is that blazars are known to show significant variability in all wavelengths and across timescales, making flux density an unreliable observable for model fitting. Instead, we only use the measured and simulated blazar flux densities to determine if a specific source would make or not the cut for inclusion in a flux-limited sample.

• *We simultaneously fit the unbeamed luminosity and bulk Lorentz factor distributions.* Since we are primarily interested in blazar timescale modulation factors in a flux-limited sample, the unbeamed luminosity function and the bulk jet Lorentz factor distribution are of equal importance in pro-

ducing the results of interest. For this reason, we want to avoid taking one of the two as input from past work and only fitting the other.

- *We focus on simplicity in both our models and our acceptability criteria.* Given that the systematic uncertainties (flux variability, redshift incompleteness, variation of component speeds within a single blazar) can be very significant, it is likely that as our understanding of blazar physics improves, our observables themselves will change, and any complex population model and/or sophisticated fit will change with them. For this reason, in this work we try to keep both the models as well as our statistical treatment as simple as possible, and our model acceptability criteria generous.

2.1 Unbeamed Luminosity Function

We assume that the jet Lorentz factor and the intrinsic, unbeamed monochromatic luminosity are uncorrelated. Expecting the blazar unbeamed luminosity function to evolve with redshift, we have adopted a pure luminosity evolution model, with a single power law between values $L_{\nu, \min}$ and $L_{\nu, \max}$ of the form

$$n(L_{\nu}, z) \propto \left(\frac{L_{\nu}}{e^{T(z)/\tau}} \right)^{-A}, \quad (1)$$

where n is the comoving number density of blazars, L is the intrinsic luminosity, τ is the evolution parameter in units of Hubble time (Padovani & Urry 1992), and $T(z)$ is the look-back time at a given redshift,

$$T(z) = \frac{1}{H_0} \int \frac{da}{a\sqrt{\Omega_m a^3 + \Omega_\Lambda}}, \quad (2)$$

where $a = (1+z)^{-1}$ is the scale factor of the Universe. We take Eq. (1) to be valid up to a maximum redshift, equal to the largest measured redshift included in our sample. At higher redshifts, we assume that the normalization of the luminosity function sharply declines with redshift. We do not implement a specific functional form for this decline, simply assuming that it is steep enough so that no higher- z source makes it into our flux-limited sample.

The probability density function (PDF) of the luminosity has the form

$$p(L_{\nu}) = C_2 \left(\frac{L_{\nu}}{e^{T(z)/\tau}} \right)^{-A}, \quad (3)$$

and the value of constant C_2 can be obtained by the requirement that the probability density integrates to 1,

$$C_2 = \frac{(-A+1)e^{-AT(z)/\tau}}{L_{\nu, \max}^{-A+1} - L_{\nu, \min}^{-A+1}}. \quad (4)$$

The cumulative density function (CDF) of this distribution is

$$\text{CDF}(L_{\nu}) = \frac{L_{\nu}^{-A+1} - L_{\nu, \min}^{-A+1}}{L_{\nu, \max}^{-A+1} - L_{\nu, \min}^{-A+1}}. \quad (5)$$

In the pure luminosity evolution model, sources become brighter with look-back time while maintaining a constant comoving number density (Padovani & Urry 1992). Then, the number of sources N in a redshift interval from z to

$z + dz$ is proportional to the comoving volume element dV ($N = ndV$), where

$$dV = \frac{c}{H_0} \frac{4\pi d_c^2 dz}{\sqrt{\Omega_m(1+z)^3 + \Omega_\Lambda}}, \quad (6)$$

and d_c is the comoving distance,

$$d_c = \frac{c}{H_0} \int_0^z \frac{dz'}{\sqrt{\Omega_m(1+z')^3 + \Omega_\Lambda}}. \quad (7)$$

2.2 Lorentz Factor Distribution

We assume a single power law of the Lorentz factor Γ of the jet is sufficient to describe any sample, as suggested by Padovani & Urry (1992) and Lister & Marscher (1997). The probability density function $p(\Gamma)$ has the form of,

$$p(\Gamma) = C_1 \Gamma^{-\alpha}, \quad (8)$$

where C_1 is a normalization constant,

$$C_1 = \frac{-\alpha + 1}{\Gamma_{\max}^{-\alpha+1} - \Gamma_{\min}^{-\alpha+1}}, \quad (9)$$

with $\Gamma_{\min} = 1$ and $\Gamma_{\max} \approx \beta_{\text{app}}^{\max}$ (Vermeulen & Cohen 1994).

2.3 Viewing Angles

We assume a random viewing angle ($\cos \theta$ uniformly distributed from 0 to 1.) Blazar jets are closely aligned with our line of sight, and we expect this to hold for the observed flux-limited sample as sources with viewing angles larger than a few degrees will not have sufficient Doppler boosting in order to pass the flux-density limit in wavelengths where blazars are the dominant AGN class.

2.4 Derived Quantities

Once the intrinsic unbeamed monochromatic luminosity L_{ν} , the bulk Lorentz factor Γ of the jet, the redshift z , and the viewing angle θ are known for a source, then we can calculate a series of derived quantities, including:

- the apparent superluminal speed of the jet,

$$\beta_{\text{app}} = \frac{\beta \sin \theta}{1 - \beta \cos \theta} \quad (10)$$

where $\beta \lesssim 1$ is the speed of the jet in units of the speed of light, which is connected to the Lorentz factor through

$$\Gamma = \frac{1}{\sqrt{1 - \beta^2}}; \quad (11)$$

- the Doppler factor,

$$D = \frac{1}{\Gamma(1 - \beta \cos \theta)}; \quad (12)$$

- the apparent timescale $\Delta t'$ of events that have a duration Δt in the jet rest frame,

$$\Delta t' = \frac{1+z}{D} \Delta t; \quad (13)$$

- and the observed monochromatic flux density,

$$S_\nu = \frac{L_\nu D^p}{4\pi d_L^2} (1+z)^{1+s}. \quad (14)$$

In Eq. (14), L_ν is the unbeamed monochromatic luminosity, $d_L = (1+z)d_c$ is the luminosity distance at a given redshift, and (s) is the spectral index, with its sign defined through $S_\nu \propto \nu^s$. The exponent p is given by $p = 2 - s$ for the continuous and $p = 3 - s$ for the discrete jet cases (Ghisellini et al. 1993). Following Lister et al. 2009b we adopt the continuous jet case ($p = 2 - s$). For FSRQs we take $s = 0.37$, (a value calculated in Lister et al. (2009b) by fitting an envelope to the β_{app} vs 15 GHz luminosity plot for MOJAVE sources); for BL Lacs we take $s = 0$ (Urry & Padovani 1991; Lister & Marscher 1997; Cohen et al. 2007).

3 SAMPLE

Our sample consists of sources with a measured redshift from the MOJAVE survey statistically complete, flux-limited sample (Arshakian, Ros & Zensus 2006; Pushkarev et al. 2009, 2012). We have excluded objects that have shown any abnormal behavior, inward motion or poor apparent velocity measurement, as indicated by Lister et al. (2009b, 2013). We also removed objects 0805-077 and 0642+449 because they were outliers, possibly indicating unique or abnormal properties: 0805-077 exhibits a far greater apparent speed than any other object ($\beta_{app} \approx 50$) and 0642+449 has an untypically high redshift ($z = 3.396$).

Our final sample consists of the 74 FSRQs and 16 BL Lacs shown in table 1 and 2 respectively.

Since we will be using MOJAVE observations at 15 GHz for the component speeds, the flux densities and luminosities we use in this work will also refer to a frequency of 15 GHz. The flux limit of our adopted sample, which we will also impose on our simulated data, is 1.5 Jy.

4 MODEL OPTIMIZATION

4.1 Observables and Model Acceptability Criteria

Sources in our adopted sample have available measurements for each of the following quantities: redshift z ; mean apparent jet speed $\langle\beta_{app}\rangle$; and average flux density $\langle S_\nu \rangle$.

In order for a model to be deemed acceptable, we require that it adequately reproduce the observed z and $\langle\beta_{app}\rangle$ distributions, when the appropriate flux limit is applied. Formally, we require a Kolmogorov-Smirnov test to return a probability higher than 5% that the simulated and observed values of z (and, similarly, of $\langle\beta_{app}\rangle$) are drawn from the same distribution.

In contrast, as discussed in §2, we do not require the model to reproduce the observed distribution of $\langle S_\nu \rangle$. We compare, however, the observed flux density distribution of the MOJAVE sample (Lister et al. 2009a) and the flux density distribution of the optimal model for the BL Lac objects and the FSRQs and discuss their agreement in §5.3. A detailed analysis of the effect of variability on the flux density distribution and the resulting fitted luminosity function will be the subject of a future publication.

The procedure for testing the acceptability of a specific model is the following:

- We use redshift bins of size 0.1 from $z = 0$ to $z = 1.4$ for the BL Lac sample and from $z = 0$ to $z = 2.5$ for the FSRQ sample. Since $dN \propto dV$ for each redshift bin, we calculate the comoving volume element and the number of repetitions performed is proportional to dV . We also calculate the proper distance for each redshift and the look-back time in order to adjust the luminosity limits in each redshift bin.
- For each repetition (simulated source), we randomly choose a value for $\cos(\theta)$, Γ , and L_ν according to the corresponding distributions of the specific model being tested.
- From these values we calculate the velocity β , the apparent velocity β_{app} , the Doppler factor D and the flux density S_ν .
- In order to simulate a flux-limited sample, we discard any source with S_ν lower than 1.5 Jy.
- We construct the cumulative distribution function of the apparent velocity and redshift distributions of simulated sources, and we compare them to those obtained from the data. We use the Kolmogorov-Smirnov test (K-S test) in order to obtain the probability of the observed and the simulated data sets having been drawn from the same distribution.

4.2 A newly optimized model

The parameters we optimize for each population are the slope A of the luminosity function, the evolution parameter τ , and the slope α of the Lorentz factor distribution. We refer to the literature (Lister & Marscher 1997) for an estimate of the power law indices for the luminosity and Lorentz factor distributions as a starting point, and proceed to explore the parameter space setting the lower limit for the luminosity to $10^{24} WHz^{-1}$ and the upper limit $10^{27} WHz^{-1}$ (Arshakian, Ros & Zensus 2006). A summary of parameter values we adopt from the literature or directly from the extrema of the datasets are shown in the upper part of Table 3.

We first perform a coarse preliminary scan of the parameter space to derive initial values for the parameters to be optimized, starting from the aforementioned literature values and shifting towards higher or lower values according to the K-S test and visual inspection of the probability density and cumulative distribution functions. During that investigation we have come to the conclusion that the luminosity function of the BL Lacs does not evolve with redshift, consistent with the recent findings of Ajello et al. (2014): the pure luminosity evolution model with a finite evolution parameter was unable to adequately describe the redshift distribution of the BL Lac objects. All the corresponding K-S test of the BL Lac redshift distribution with an evolution parameter close to the literature value gave probabilities $\leq 10^{-5}\%$ of consistency. The probability values increased while increasing the value of the evolution parameter, and reached acceptable levels, as described in §4.1, when the evolution parameter was set to infinity.

Starting from the initial values obtained in our coarse scan, we optimize the model parameters in the following way. We create a 3-dimensional cube in parameter space for the FSRQS (A, τ, α) and a 2-dimensional plane for the BL

Table 1. FSRQS sample

Object Name	β_{app}	Redshift	Object Name	β_{app}	Redshift
0016+731	6.74	1.781	1219+044	2.35	0.965
0059+581	8.705	0.644	1222+216	15.882	0.432
0106+013	24.04	2.099	1226+023	9.643	0.158
0119+115	17.1	0.570	1334-127	6.99	0.539
0133+476	11.5	0.859	1417+385	15.4	1.831
0202+149	6.4	0.405	1458+718	3.907	0.904
0202+319	4.686	1.466	1502+106	10.2	1.839
0212+735	4.87	2.367	1504-166	3.413	0.876
0215+015	18.466	1.715	1510-089	16.11	0.360
0224+671	5.895	0.523	1546+027	8.5675	0.414
0234+285	12.12	1.207	1548+056	7.7	1.422
0333+321	12.2	1.259	1606+106	17.1	1.226
0336-019	13.07	0.852	1611+343	7.69	1.397
0420-014	5.6	0.914	1633+382	16.6625	1.814
0458-020	15.045	2.286	1637+574	9.07	0.751
0528+134	11.036	2.070	1638+398	8.266	1.666
0529+075	8.325	1.254	1641+399	12.4175	0.593
0529+483	17.54	1.162	1726+455	1.873	0.717
0552+398	0.363	2.363	1730-130	17.622	0.902
0605-085	16.186	0.872	1751+288	3.07	1.118
0730+504	12.75	0.720	1800+440	15.04	0.663
0736+017	9.332	0.191	1849+670	22.1	0.657
0738+313	6.986	0.631	1928+738	4.774	0.302
0748+126	14.365	0.889	1936-155	2.6	1.657
0804+499	1.83	1.436	1958-179	1.9	0.650
0827+243	17.7675	0.940	2037+511	3.3	1.686
0836+710	19.35	2.218	2121+053	10.845	1.941
0838+133	8.223	0.681	2136+141	3.7975	2.427
0906+015	19.645	1.024	2145+067	2.206	0.990
0923+392	2.44	0.695	2155-152	12.66	0.672
0945+408	13.256	1.249	2216-038	5.55	0.901
0955+476	2.48	1.882	2223-052	13.0425	1.404
1036+054	6.065	0.473	2227-088	8.1	1.560
1038+064	7.26	1.265	2243-123	3.88	0.632
1045-188	6.085	0.595	2251+158	7.27	0.859
1150+812	5.878	1.250	2331+073	3.445	0.401
1156+295	20.15	0.729	2345-167	11.21	0.576

Mean β_{app} from Lister et al. (2009b); redshifts from Lister et al. (2009a).

Table 2. BL Lac sample

Object Name	β_{app}	Redshift	Object Name	β_{app}	Redshift
0003-066	2.145	0.347	1413+135	0.755	0.247
0716+714	10.07	0.310	1538+149	4.525	0.605
0754+100	14.4	0.266	1749+096	4.013	0.322
0808+019	13.000	1.148	1803+784	2.396	0.680
0814+425	1.060	0.245	1807+698	0.056	0.051
0823+033	14.3	0.506	1823+568	7.225	0.664
0829+046	6.347	0.174	2131-021	10.318	1.285
0851+202	8.613	0.306	2200+420	5.1335	0.068

Mean β_{app} from Lister et al. (2009b); redshifts from Lister et al. (2009a).

Lacs (A, α). Each side of the cube is centered in the corresponding parameter value generating the smallest inconsistency between observed and simulated cumulative distribution functions, and its extent is equal to the coarse-scan step.

For each sample, we take every possible combination of parameters and choose the one that minimizes the com-

bined inconsistency between the observed and simulated cumulative distribution functions of the β_{app} and redshift distributions (we quantify that “combined inconsistency” by the product of the corresponding K-S test statistics). We then repeat the process three additional times, adjusting the boundary values to the step of the previous scan, and using smaller steps centered around the previously obtained

Table 3. Model Parameters. Upper part: model values adopted from the literature or directly from extrema of observable distributions (see text). Lower part: optimal parameter values; spread represents scanning step and statistical variations in simulated distributions. The second asymmetrical errors represent the range within which a parameter can produce "acceptable models"

	BL Lacs	FSRQs
Γ_{min}	1	1
Γ_{max}	16	26
$L_{min}(\text{W Hz}^{-1})$	10^{24}	10^{24}
$L_{max}(\text{W Hz}^{-1})$	10^{27}	10^{27}
s	0	0.37
α	$0.738 \pm 0.002^{+0.41}_{-1.46}$	$0.57 \pm 0.001^{+0.12}_{-0.50}$
A	$2.251 \pm 0.02^{+0.68}_{-0.78}$	$2.6 \pm 0.01^{+0.185}_{-0.245}$
$\tau(1/H_0)$	-	$0.26 \pm 0.001^{+0.068}_{-0.003}$

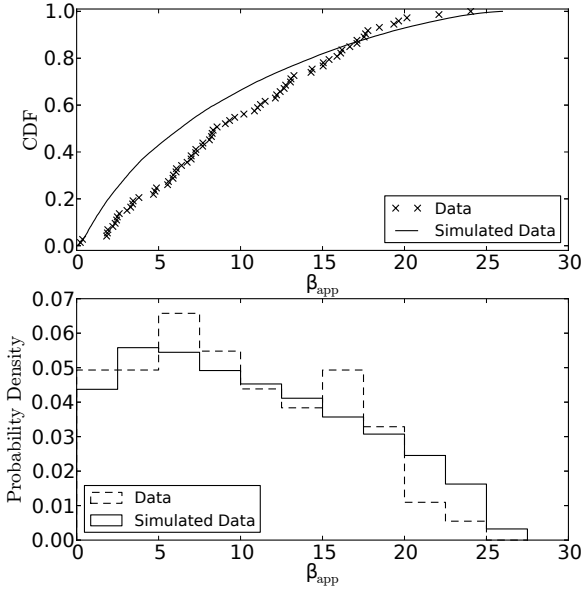


Figure 1. Cumulative distribution function (upper panel) and probability density function (lower panel) of simulated (with our optimal model) and observed (MOJAVE sample, see text) β_{app} for FSRQs.

optimal parameters, in order to converge to the best result. In order to investigate the effects of random sampling and account for statistical deviations, we repeat several times the final scan. The optimal parameters values are shown in the lower part of Table 3. Values and error bars correspond to the average and the spread (standard deviation) of the various incarnations of the final-scan optimization. They are therefore representative of the statistical spread in simulated distributions (and indicative of the step in our final scan). In contrast, the range of parameters that produce simulated distributions consistent with the observable ones is addressed later in this section. For the FSRQ optimal parameters, the K-S test p-values are 49.3% for the apparent

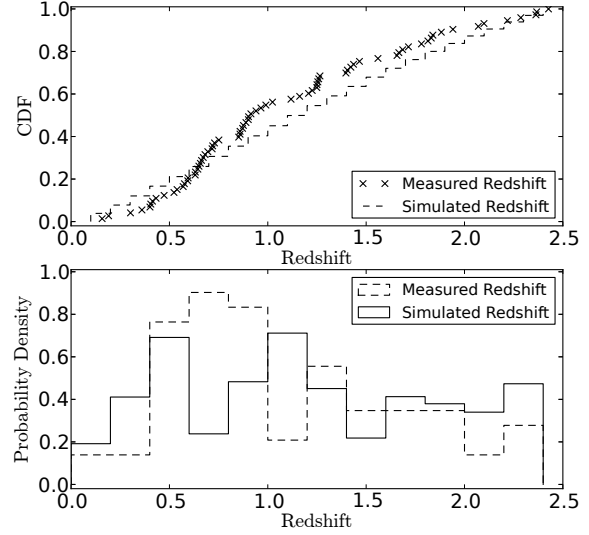


Figure 2. Cumulative distribution function (upper panel) and probability density function (lower panel) of simulated (with our optimal model) and observed (MOJAVE sample, see text) redshifts z for FSRQs

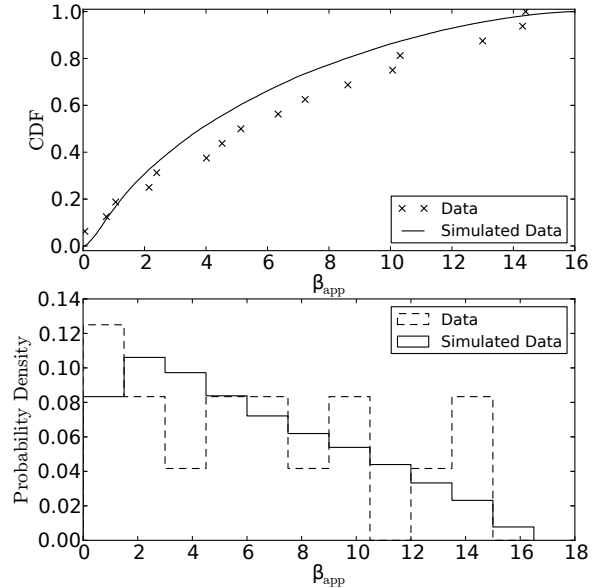


Figure 3. Cumulative distribution function (upper panel) and probability density function (lower panel) of simulated (with our optimal model) and observed (MOJAVE sample, see text) β_{app} for BL Lacs

velocity and 8.4% for the redshift distributions (see also Fig. 1,2). For the BL Lac optimal parameters, the corresponding K-S test p-values of 93.4% for the apparent velocity and 54.1% for the redshift distributions (see also Fig. 3,4).

It should be noted that the optimization procedure does not formally correspond to proper model fitting that could be achieved, for example, using a maximum-likelihood anal-

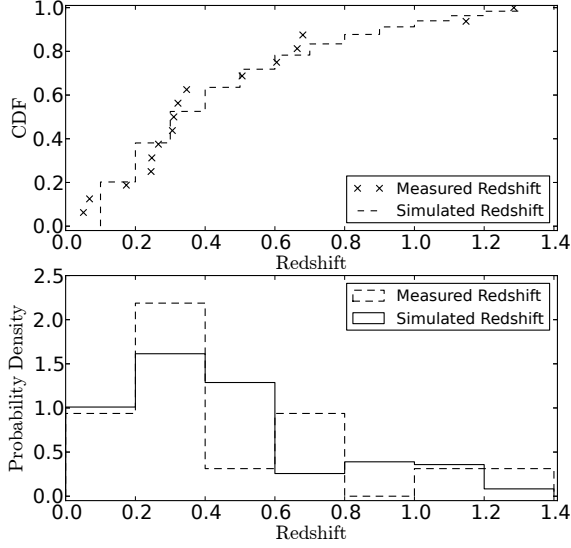


Figure 4. Cumulative distribution function (upper panel) and probability density function (lower panel) of simulated (with our optimal model) and observed (MOJAVE sample, see text) redshifts z for BL Lacs.

ysis, or a chi-square minimization of the simulated probability density functions on the observed ones. There are two reasons we have instead adopted the simpler procedure described here and which is based on the K-S statistic. The first one is simplicity. As discussed in §2, systematic uncertainties in the observables and their interpretation are expected to be significant, and affect the optimal model parameters much more than the details of the optimization procedure. For this reason, the investment in algorithmic complexity and computational time will likely not yield a proportional improvement in model accuracy. The second reason is that the K-S statistic provides an automatic way to assess model consistency with the data: a nominal fitting procedure will yield the model parameters *in best agreement* with the data, without any a priori guarantees that this family of model is a *good* (or even acceptable) description of that dataset. Our procedure however allows us to automatically reject poor fits up to a desired K-S p-value level and find the range of parameters (if such a range exists) for which the hypothesis that the chosen family of models produces the observed dataset cannot be rejected.

In order to determine that range that produces “acceptable models” for each parameter, we create a 2-D (for the BL Lacs), and a 3-D (for the FSRQs) parameter space centered around the best-fit values for each model. We use Monte Carlo sampling of the parameter space, to test which combination of parameters produce “acceptable” models, i.e. the K-S test yields a $\leq 5\%$ probability of consistency between observed and simulated distributions. We repeat this process enough times in order to ensure that the parameter space is adequately sampled. The range of parameter values produced in this way represents the spread of each parameter. If the extrema of these values coincide with the extrema of the initial parameter space, we increase the range of that space and repeat the process. For the FSRQs this procedure yields

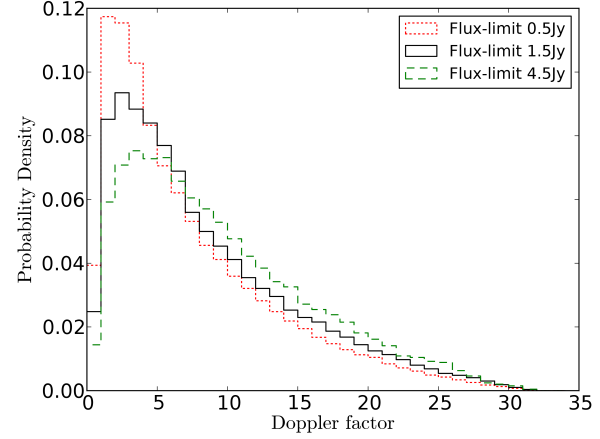


Figure 5. BL Lac Doppler factor distribution. Different line types corresponds to different flux limits as follows. Solid line: 1.5 Jy; dashed line: 4.5 Jy; dotted line: 0.5 Jy.

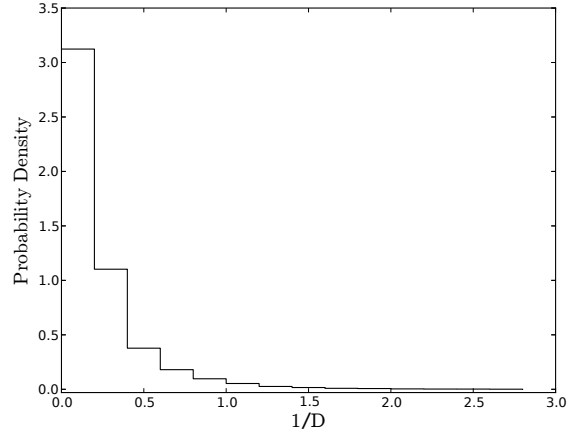


Figure 6. Inverse Doppler factor distribution for a flux limited ($S_\nu \geq 1.5$ Jy) BL Lac sample.

$\alpha = 0.57^{+0.12}_{-0.50}$, $A = 2.6^{+0.185}_{-0.245}$, $\tau = 0.26^{+0.068}_{-0.003}$. For the BL Lacs the procedure yields $\alpha = 0.738^{+0.41}_{-1.46}$, $A = 2.251^{+0.68}_{-0.78}$.

5 RESULTS

5.1 BL Lacs

Using the optimal values for the two parameters of our BL Lac population model, we explore, in this section, the distributions of the derived quantities discussed in §2. The Doppler factor distribution and inverse Doppler, which will be important in the application to the timescale analysis, are shown in Fig. 5 & 6. The distribution of the viewing angles for sources that pass the flux limit is shown in Fig. 7, and the distribution of the product ($\Gamma\theta$) in Fig. 8.

We can clearly see in Fig. (7) that the sources that manage to pass the flux limit are strongly biased towards very small viewing angles, consistent with our understanding of blazars having jets closely aligned with our line of sight.

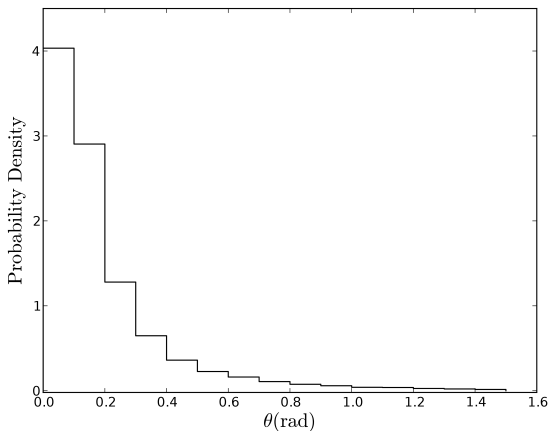


Figure 7. Distribution of the viewing angles θ (rad) for a flux limited ($S_\nu \geq 1.5$ Jy) BL Lac sample. The majority of simulated sources have small viewing angles (68.8% have $\theta \leq 0.2$ rad = 11.5°), in accordance with our understanding of blazars.

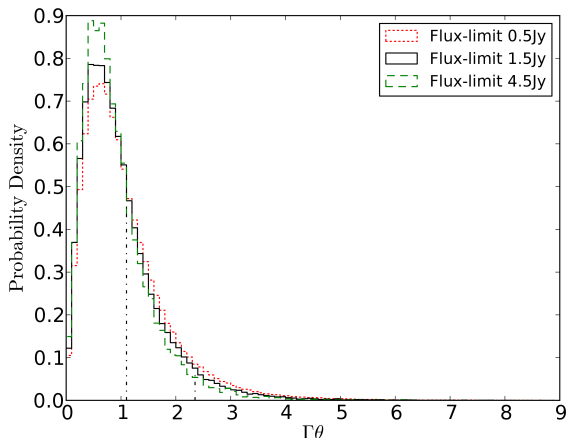


Figure 8. Distribution of $\Gamma\theta$ for flux-limited BL Lac samples. Different lines correspond to different flux limits as follows. Solid line: 1.5 Jy; dashed line: 4.5 Jy; dotted line: 0.5 Jy. The vertical dashed line at 1.11 represents 1σ , at 2.37σ and the dashed line (not visible at $\Gamma\theta = 4.8$) 3σ for the 1.5 Jy distribution.

Although most sources in the inverse Doppler factor distribution have $1/D < 1$ (Fig. 5), there is a non-zero power at $1/D > 1$. All sources with $1/D > 1$ are not boosted.

The optimal parameters presented in Table 3 are applicable to the entire BL Lac distribution. In contrast, the resulting derivative-quantity distributions presented in this section are specific to a sample (characterized by a certain flux limit). To demonstrate this explicitly, we plot, in Figs. 5 and 8, the resulting distributions (D and $\Gamma\theta$) if we implement a different flux limit. We choose to use limits a factor of 3 higher (4.5 Jy) and lower (0.5 Jy) than the limit of the observed dataset (1.5 Jy). In both cases we see that the distributions have similar shapes, and the location of their peaks are insensitive to the flux limit; however, the power in the tails compared to the peak changes as the value of the flux limit changes. As expected, the Doppler factor dis-

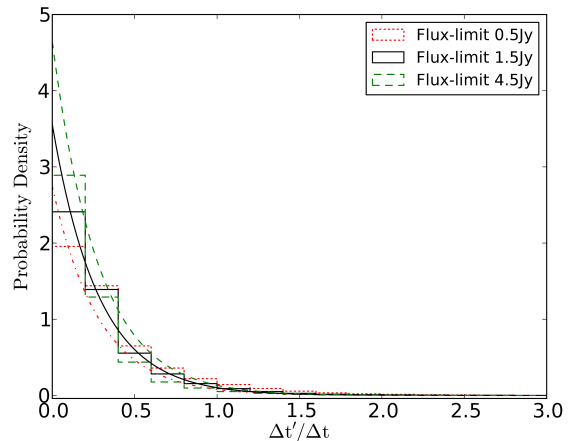


Figure 9. Time scale modulation factor distribution for BL Lac objects. Different line types correspond to different flux limits as follows. Solid line: 1.5 Jy; dashed line: 4.5 Jy; dotted line: 0.5 Jy. The overplotted smooth lines represent exponential distributions with the same mean as each histogram.

tribution has more power in the tails (a larger fraction of highly boosted sources) as the flux limit increases. The $\Gamma\theta$ distribution shows an increase in the number of sources with lower values (more highly beamed sources) as the flux limit increases. We therefore emphasize that although our optimized Γ and L_ν distributions describe blazars as a population, the correct flux limit must be taken into account when using them to obtain distributions of derivative quantities to compare with a specific flux-limited sample.

It is common in studies of beamed sources, when there is not enough information to estimate both Γ and θ for a source, to assume an average value of $\Gamma\theta$ (typically, $\Gamma\theta = 1$, e.g. Vermeulen 1995; Cohen et al. 2007). The preference for $\Gamma\theta = 1$ stems from the fact that, if the Lorentz factor associated with the observed movement of the knots in a jet is also the Lorentz factor of the bulk flow, then the maximum apparent speed for a given Γ is achieved for $\sin\theta = 1/\Gamma$. Thus for small angles $\theta \sim 1/\Gamma$. Figure 8 allows us to evaluate the validity of that assumption. The most likely value of $\Gamma\theta$ is at 0.6 (see also Jorstad et al. 2005), and this result is quite robust with respect to the sample flux limit. The mean for $S_\nu \geq 1.5$ Jy is 0.95, close to the frequently assumed $\Gamma\theta$ value. However, we point out that the spread of the $\Gamma\theta$ distribution is large: 68% of all values are included between $0 \leq \Gamma\theta \leq 1.1$. For this reason, any assumption regarding the value of $\Gamma\theta$, whether that value is the mean or the mode of the simulated distributions, should be treated with caution.

The emission from a region with bulk relativistic Lorentz factor Γ is generally beamed within a cone of opening angle $1/\Gamma$. For this reason, for beamed sources we expect $\Gamma\theta < 1$. Due to the spread of the distribution, we conclude that most, but not all, of the sources in a flux-limited sample of relativistic jets are beamed.

Combining the Doppler factor and redshift distributions (Eq.13) we derive the timescale modulation factor distribution (Fig. 9). The distribution can be well described by an exponential distribution with mean equal to the data mean. In the case of a flux limit of 1.5 Jy, the mean timescale mod-

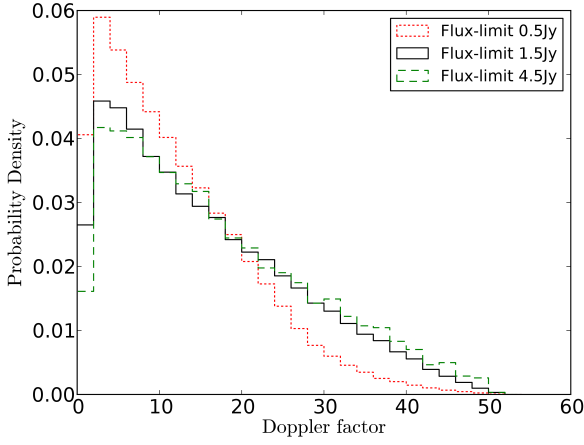


Figure 10. Doppler factor distribution for FSRQs. Different line types correspond to different flux limits, as follows. Solid line: 1.5 Jy; dashed line: 4.5 Jy; dotted line: 0.5 Jy.

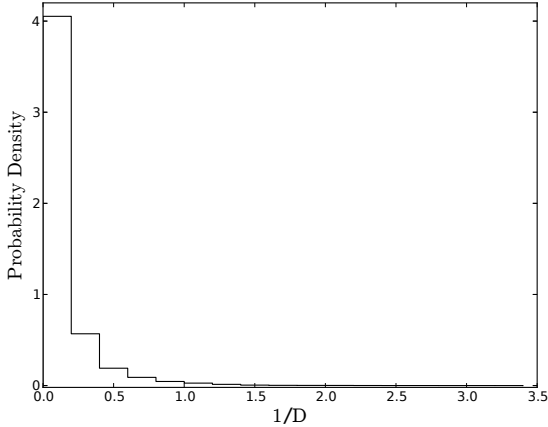


Figure 11. Inverse Doppler factor distribution for the FSRQs sample.

ulation factor is equal to 0.281. However, the distribution is not a strict exponential, because the maximum Doppler factor is finite and hence the time modulation factor is never exactly equal to zero. Its smallest value in the $S_\nu \geq 1.5 \text{ Jy}$ sample is $\sim 3 \times 10^{-2}$. In Fig. 9 we also plot the resulting distributions if we implement a different flux limit, as in Figs. 5 and 8. Higher flux limits result to a larger fraction of sources with very compressed timescales.

5.2 Flat spectrum Radio Quasars

In this section, we discuss the same derived distributions for FSRQs as the ones we derived for BL Lacs in §5.1. The Doppler and inverse Doppler factor distribution and the distribution of the viewing angles are shown in Figs. 10, 11 and 12 respectively. The Doppler factor distributions of the BL Lac and FSRQ samples show remarkable similarities. Even though FSRQs have higher Doppler factors, both distributions peak at ~ 3 and have similar shapes.

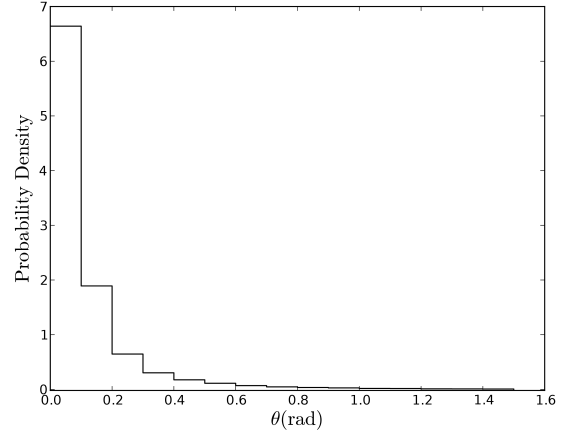


Figure 12. Distribution of the viewing angles $\theta(\text{rad})$. The majority of simulated sources have small viewing angles (85% have $\theta \leq 0.2 \text{ rad} = 11.5^\circ$), in accordance with our understanding of blazars.

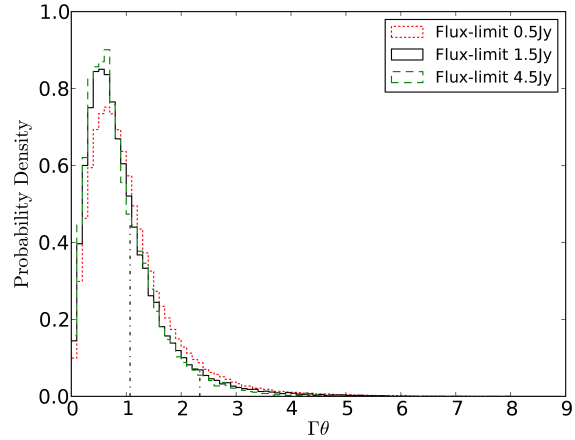


Figure 13. Distribution of $\Gamma\theta$ for the FSRQ sample. The solid line represents the distribution with the flux limit we set for our model (1.5 Jy). The dashed line is the distribution for a flux limit of 4.5 Jy and the dotted line for a limit of 0.5 Jy. The vertical dashed line at 1.07 represents 1σ , at 2.34 2σ and the dashed line (not visible at $\Gamma\theta = 5.0$) 3σ for the 1.5 Jy distribution.

The distribution of the $(\Gamma\theta)$ is shown in Fig. 13. As in the case of BL Lacs, we find the $\Gamma\theta$ to be peaked around 0.5, in agreement with the early analytic predictions of Vermeulen & Cohen (1994) for quasars. The consistency between the $\Gamma\theta$ distributions in FSRQs and BL Lacs is remarkable; differences in the amount of relativistic beaming are not likely to be the culprit of any observed differences between these two classes of sources.

The same conclusion can be reached by comparing the time scale modulation factor distribution for the FSRQs, shown in Fig. 14, with that of BL Lacs. The time scale modulation factors of a 1.5 Jy flux-limited FSRQ sample also follow an exponential distribution with mean = 0.277. Similar to the BL Lacs, the smallest value is $\sim 2 \times 10^{-2}$.

As for BL Lacs, we have also produced distributions for

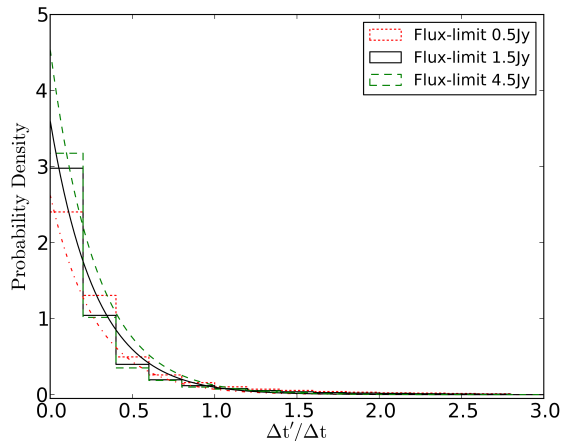


Figure 14. Time scale modulation factor distribution of the simulated data for the FSRQ sample. The solid line represents the distribution with the flux limit we set for our model (1.5 Jy). The dashed line is the distribution for a flux limit of 4.5 Jy and the dotted line for a limit 0.5 Jy. The overplotted lines represent exponential distributions with the same mean.

the Doppler factor, $\Gamma\theta$ and the time scale modulation factor for samples with different flux limits. The effect of changing the flux limit is similar for the FSRQs as in the case of BL Lacs. In all three cases the distributions have similar peaks, and the Doppler factor distribution becomes shallower with higher flux limit, whereas more sources have smaller values of $\Gamma\theta$ and $\Delta t'/\Delta t$ for a higher flux limit.

5.3 Flux density and Luminosity Distributions

It was argued in §4.1 that due to the variable nature of blazars, flux density is not a good observable for model fitting. For this reason, we have not required that our acceptable models produce a flux density distribution consistent with the data. It is nevertheless interesting to compare, the flux density distributions in our simulated and observed 1.5Jy flux-limited samples. Figures 15 & 16 show the distribution of the derived flux density versus the highest flux density from observations (Lister et al. 2009a) for the BL Lac and FSRQ samples respectively. Despite our initial concerns regarding variability, simulated and observed distributions do not appear to be discrepant in either case. The Kolmogorov-Smirnov test gives a probability of $\sim 23\%$ for the BL Lac objects and $\sim 21\%$ for the FSRQs that the observed and simulated data are drawn from the same distribution. A possible interpretation of this result is that the probability of observing a source in a flaring state in a single-epoch survey is low. Lister (2001) has argued that even though the flux densities of beamed sources can reach high levels because of Doppler boosting, compression of flare timescales implies that these sources are most likely to be observed relatively close to their quiescent levels.

Figure 17 shows the flux density distribution of the two samples in the $\log N - \log S_\nu$ format. The flux density distribution of the sources above the 1.5Jy flux limit follows a power law distribution with a slope of -2.2 for the BL Lacs and -2.6 for the FSRQs. For comparison, a uniformly dis-

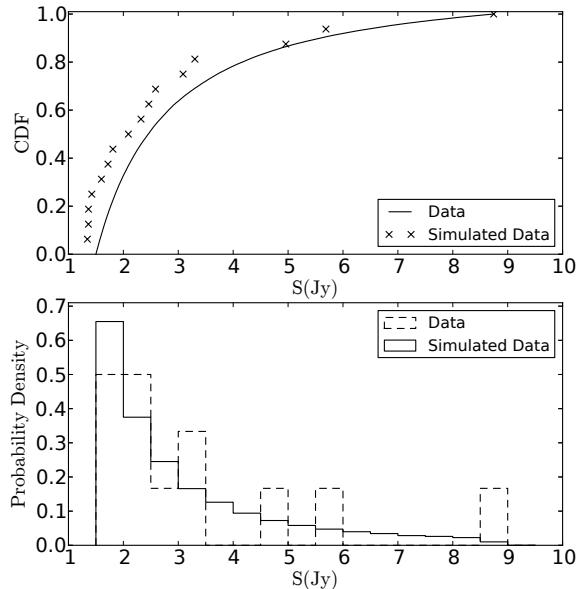


Figure 15. Flux density distribution of the MOJAVE sample (BL Lacs) (Lister et al. 2009a)(dashed) and the simulated flux density (solid).

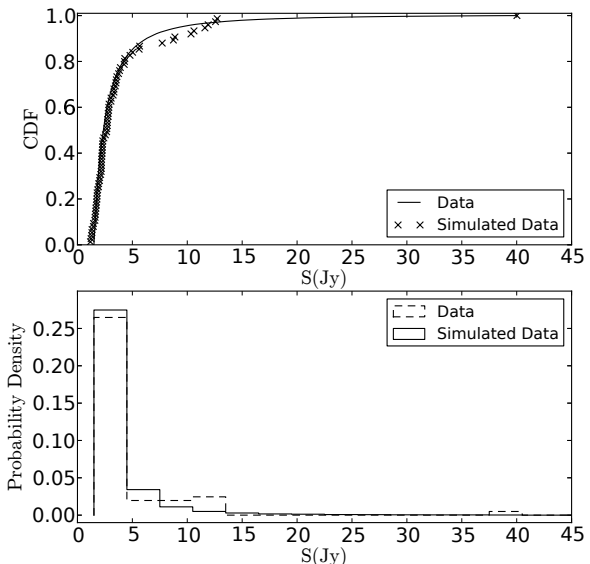


Figure 16. Flux density distribution of the MOJAVE sample (FSRQs) (Lister et al. 2009a)(dashed) and the simulated flux density (solid).

tributed, single-luminosity extragalactic population in a flat cosmology yields a slope of -2.5.

The $\log N - \log L_\nu$ plots for unbeamed and beamed luminosities of the sources that pass the 1.5 Jy flux limit are shown in Figs. 18 and 19 respectively. For the unbeamed case we have also overplotted the input intrinsic luminosity functions at $z=0$. As expected, the intrinsic distribution of

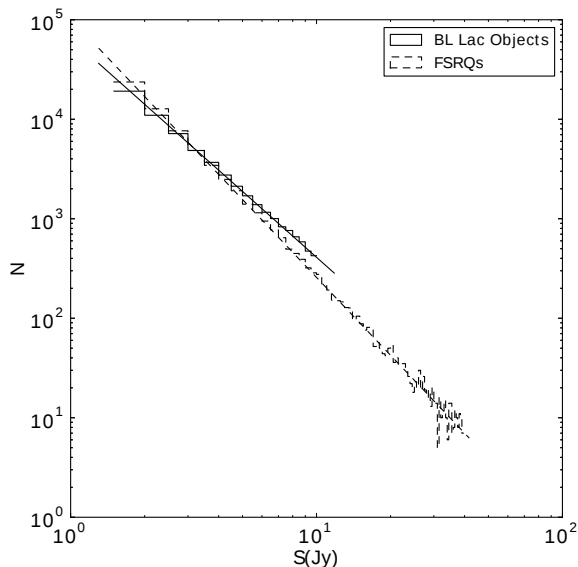


Figure 17. $\log N$ - $\log S_\nu$ plot for the FSRQ (dashed) and BL Lac (solid) 1.5 Jy - limited samples. The corresponding lines represent power law distributions with slope -2.2 for the BL Lac objects and -2.6 for the FSRQs.

the luminosity is steeper than the distribution of the luminosity of the sources above the flux limit for both samples (e.g. Cara & Lister 2008a).

In the case of the beamed luminosity functions we see a clear break in the beamed $\log N$ - $\log L_\nu$ of the FSRQ sample at $\sim 2 \times 10^{28} \text{ W Hz}^{-1}$ and a less pronounced break in the beamed $\log N$ - $\log L_\nu$ of the BL Lac sample.

The deviations from a single power law in the distribution of luminosities *within the sample* are not a reflection of the intrinsic luminosity function shape (which, in our case, is a single power-law by construction). Rather, they are artifacts of beaming (see also Urry & Shafer 1984; Urry & Padovani 1991) and mixing objects from different redshifts; for example, the sources above and below the break in the case of FSRQs are strongly dominated by objects at redshifts higher and lower than ~ 1 , respectively. However, past studies have shown that reconstruction of the luminosity function starting from observations in a flux-limited sample can erroneously map these breaks to the intrinsic luminosity function shape (Cara & Lister 2008b,a). Our results do not show any need for a blazar luminosity function shape more complex than a single power law.

6 SUMMARY AND CONCLUSIONS

Using a Monte Carlo approach, we produced a new statistical model for the blazar population, parameterized by the power law indexes of the luminosity and Lorentz factor distributions, and the evolution parameter. We derive distinct distribution parameters for FSRQs and BL Lacs. Using this model we can produce distributions for the Doppler factor, viewing angle, product $\Gamma\theta$, and time scale modulation factor for any flux-limited sample of beamed sources.

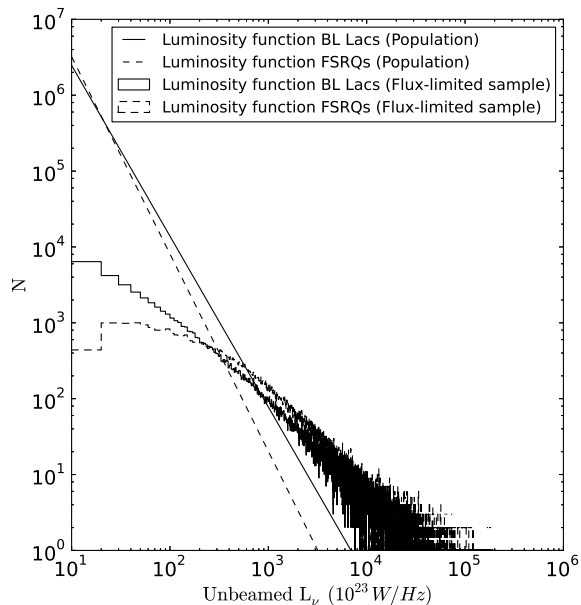


Figure 18. Unbeamed $\log N$ - $\log L_\nu$ for the FSRQ (dashed) and BL Lac (solid) 1.5 Jy - limited samples. The solid and dashed lines represent the input power law distribution at $z=0$ for the BL Lac and the FSRQ samples respectively.

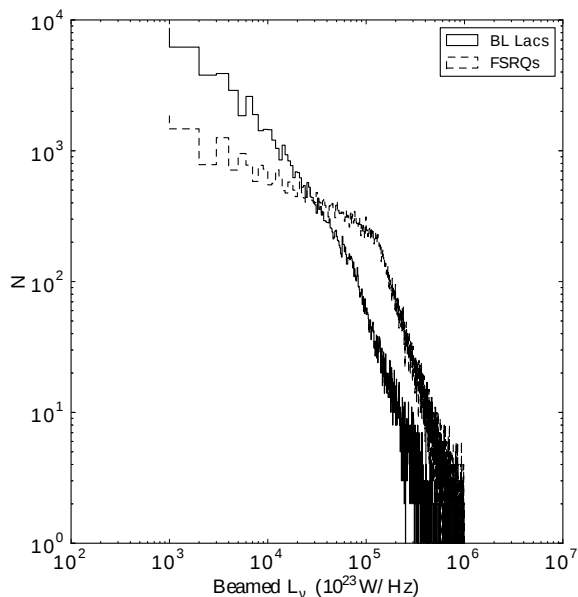


Figure 19. Beamed $\log N$ - $\log L_\nu$ for the FSRQ (dashed) and BL Lac (solid) 1.5 Jy - limited samples.

We have set out with the aim to answer the following three questions regarding the blazar population.

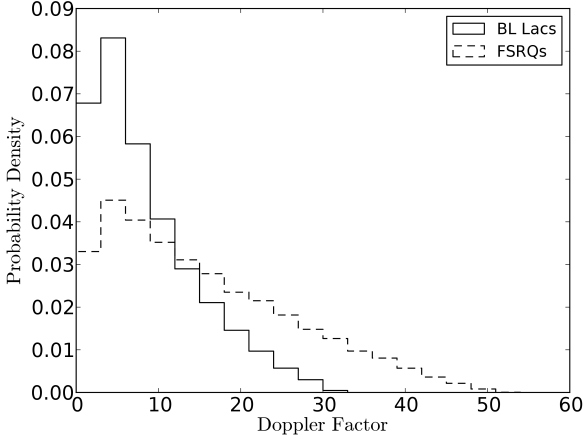


Figure 20. Distributions of Doppler factors for the BL Lac (solid) and the FSRQ (dashed) 1.5 Jy - limited samples

6.1 What is the relativistically induced spread in observed event timescales?

Because of relativistic and cosmological expansion effects, even events with identical timescales across sources would appear to have a distribution of observed timescales, as long as the members of the sample we are considering have a variety of Doppler factors (Fig. 20) and/or redshifts (Fig. 2,4). We can quantify this spread by considering the simple case where indeed we have a class of events with identical rest-frame timescales $\tau_r = T$ across all sources, and calculating the resulting distribution of observed timescales.

Defining the timescale modulation factor $m = \Delta t' / \Delta t$, τ_r is related to the observed timescale τ_o through $\tau_o = m\tau_r$. The distribution of τ_r is a delta function,

$$p(\tau_r) = \delta(\tau_r - T). \quad (15)$$

We have shown that the distribution of m is an exponential,

$$p(m) = C \frac{1}{m_0} \exp \left[-\frac{m}{m_0} \right], m_{\min} \leq m \leq m_{\max} \quad (16)$$

where C is a normalization constant to account for the truncated range. If m and τ_r are independent, their joint probability function is

$$p(m, \tau_r) = C \frac{1}{m_0} \exp \left[-\frac{m}{m_0} \right] \delta(\tau_r - T) \quad (17)$$

within the same limits as above. Transforming to new variables m, τ_o and integrating over all values of m we obtain

$$p(\tau_o) \propto \exp \left[-\frac{\tau_o}{T m_0} \right]. \quad (18)$$

Inverting this problem, we conclude that the observation of an exponential distribution of timescales associated with a class of events in a flux-limited sample of BL Lacs or of FSRQs is consistent with all timescales being identical in the rest frame of the jet. The jet rest-frame timescale of such a class of events is equal to the observed mean timescale divided by the average timescale modulation factor of the relevant sample.

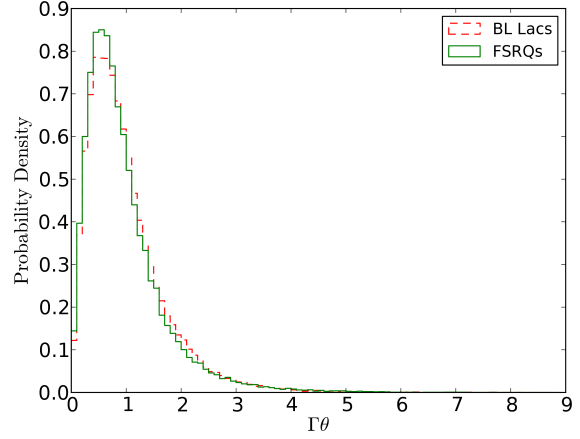


Figure 21. Distributions of $\Gamma\theta$ for the BL Lac (dashed) and the FSRQ (solid) 1.5 Jy - limited samples

6.2 Beaming of sources in flux-limited samples.

In any flux-limited sample there is a well-defined peak in the probability distribution of $\Gamma\theta$, and the location of this peak is rather robust with respect to the value of the flux limit (0.6 for BL Lacs, 0.5 for FSRQs Fig. 21). The mean of this distribution is closer to 1 (0.99 for BL Lacs, 0.95 for FSRQs). As is indicated by the significant difference between mode and mean, the distribution is not only skewed but also its spread is large. Indeed, for a 1.5 Jy - limited sample, 68% of sources are contained in the interval $0 \leq \Gamma\theta \leq 1.11$, and 95% of sources between 0 and 2.37. The consequence is that, lacking enough information to compute both Γ and θ for a source, it is precarious to make a statistical assumption for the value of $\Gamma\theta$ in order to close the system and solve the problem. If any such assumption is made, the 1σ uncertainty places the value of $\Gamma\theta$ between 0 and 1.1, i.e. maximally beamed and marginally beamed.

For this reason, although the amount of beaming for a large sample of sources can be usefully constrained through models of the type discussed here, we strongly recommend against using such statistical arguments on single sources.

6.3 BL Lacs and FSRQs do NOT have different beaming properties.

Although BL Lacs have a steeper optimal slope in their Γ distribution, lower values of Γ (Fig. 22), and larger, on average, viewing angles (Fig. 23), than FSRQs, the distributions of the quantities characterizing beaming and timescale compression ($\Gamma\theta$ and $\Delta t' / \Delta t$, respectively), are very similar. The monoparametric exponential distributions that can describe the latter have consistent mean: for the 1.5 Jy - limited sample and our optimal model, these are 0.281 for the BL Lacs and 0.277 for the FSRQs.

The consequence of this result is that any difference observed between BL Lac and FSRQ flux-limited samples (with the same flux limit) in the time domain are not due to differences in relativistic timescale compression between the two classes. Rather, they must be reflecting an intrinsic difference between these two classes of sources.

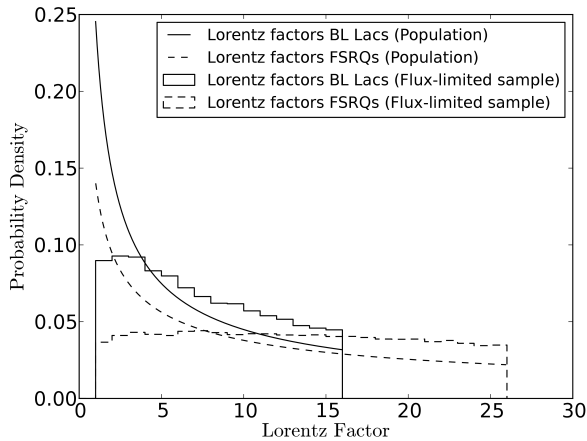


Figure 22. Distributions of Lorentz factors for the FSRQ (dashed) and BL Lac (solid) 1.5 Jy - limited samples. The solid and dashed lines represent the input power law distribution for the BL Lac and the FSRQ samples respectively.

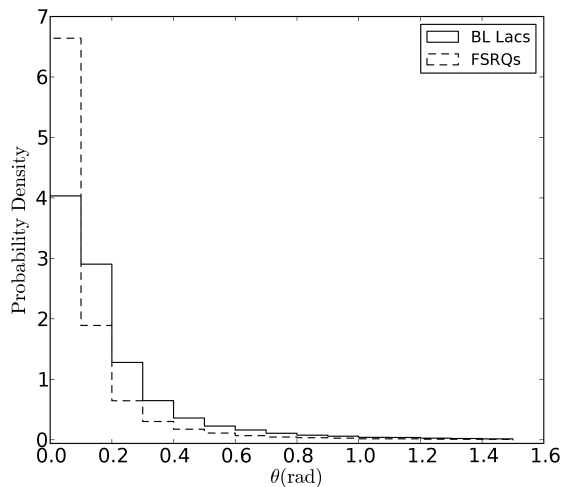


Figure 23. Distributions of viewing angles for the BL Lac (solid) and the FSRQ (dashed) 1.5 Jy - limited samples.

There is some uncertainty in this result stemming from uncertainty in our distribution parameters. In order to quantify this effect, we calculate the mean of $\Delta t'/\Delta t$ in a 1.5 Jy - limited sample for different values of the input distribution parameters. As in §4.2, we have kept all but one parameters at their optimal values, and varied the remaining one to the limit (maximum and minimum) where it still produces acceptable z and β_{app} distributions (K-S test better than 5%). The values of the limiting parameter values are given in §4.2, and the corresponding values of the $\Delta t'/\Delta t$ means are given in Table 4. The largest possible deviation from our optimal parameter values is produced for shallower luminosity function slopes in BL Lacs.

Table 4. Model Parameters

Parameters	$\langle \Delta t'/\Delta t \rangle_{\text{BL Lacs}}$	$\langle \Delta t'/\Delta t \rangle_{\text{FSRQs}}$
α_{\min}	0.167	0.208
α_{\max}	0.344	0.303
A_{\min}	0.559	0.426
A_{\max}	0.143	0.204
τ_{\min}	-	0.282
τ_{\max}	-	0.246
Optimal	0.281	0.277

7 DISCUSSION

We have made a point of optimizing different models for BL Lacs and FSRQs. An evaluation of whether this is indeed a necessary distinction can be made after the fact, by comparing the optimal models between BL Lacs and FSRQs. We find that FSRQs are:

- **Faster:** BL Lacs statistically have lower Lorentz factors than FSRQs, as their Γ -distribution is steeper (Fig. 22).
- **Evolving:** we have found that the luminosity distribution of FSRQs moves to higher luminosities with increasing redshift; conversely, the BL Lac redshift distribution with a luminosity function that evolves with redshift. In principle, this result could be affected by the redshift incompleteness of the BL Lac sample, which is larger than that of the FSRQ sample, if lower redshifts are preferentially easier to measure. However, there is no evidence for any evolution *even among lower redshifts* (for example from $z = 0$ to $z = 0.4$, where one would not expect to have our ability to measure redshifts to vary dramatically). If such a bias exists, it would have to be rather fine-tuned to exactly match the brightening of higher-redshift sources. This finding is consistent with gamma-ray studies of the BL Lac luminosity function (Ajello et al. 2014).
- **Brighter:** Even though today BL Lacs are brighter than FSRQs (Fig.19), the situation is reversed at higher redshifts, due to the evolution of FSRQs.

It is therefore particularly interesting that, despite their intrinsic differences, these two classes appear to have very consistent relativistic beaming ($\Gamma\theta$ distribution serves as a proxy) and timescale compression distributions in flux-limited samples. Their intrinsic differences are thus expected to be imprinted in their statistical properties in the time domain measured in the observer frame.

Throughout this work we have assumed a single value for the spectral index (s) for all sources in each sample. In reality it is different for every source and can evolve with time (Angelakis et al. 2012; Hovatta et al. 2014). However, since this simple assumption has yielded adequate results, we have not treated separately a spectral index distribution, although such an extension could be added to our model in a straight-forward fashion.

Single power law distributions for the Lorentz factors and the luminosity function are sufficient to describe both samples: the K-S test values for the FSRQs are 49.3% for the apparent velocity and 8.4% for the redshift distributions while for the BL Lacs 93.4% for the apparent velocity and 54.1% for the redshift distributions.

We have calculated, and we quote, mean values of the timescale modulation factor, for a 1.5 Jy flux-limited sample. Since we have shown that this distribution can be well-described by an exponential, the mean is the only parameter needed to completely define it. However, we emphasize that the value of the mean is a quantity dependent on the flux limit. Applications to different samples need to properly calculate the distribution appropriate to the relevant flux limit.

In addition we caution the reader that results of our models for lower flux limits involve extrapolation and should thus be treated with caution.

In this work, we have treated BL Lacs and FSRQs separately. The small number of BL Lacs make the BL Lac sample and the associated results more sensitive to contamination borderline shifting classification sources. However, it is striking that even with such a small sample, no agreement with even a mildly evolving luminosity function was possible.

The model optimized here was based on 15 GHz radio data. Any application to the statistical interpretation of data obtained in other frequencies should be done with two possible caveats in mind. First, it is not necessarily obvious that a single Lorentz factor can characterize the jet at all frequencies, or even at all locations at the same frequency (e.g., Georganopoulos & Kazanas 2004). Second, a flux-limited sample at a different frequency range (e.g., gamma-ray or optical), does not translate directly to a flux-limited sample in radio (e.g., Pavlidou et al. 2012). The scatter in the correlation between fluxes at different frequencies must therefore be accounted for.

ACKNOWLEDGMENTS

We would like to thank Matt Lister, Talvikki Hovatta, and the anonymous referee for comments that helped improve this work.

This research was supported by the “Aristeia” Action of the “Operational Program Education and Lifelong Learning” and is co-funded by the European Social Fund (ESF) and Greek National Resources, and by the European Commission Seventh Framework Program (FP7) through grants PCIG10-GA-2011-304001 “JetPop” and PIRSES-GA-2012-31578 “EuroCal”. This research has made use of data from the MOJAVE database that is maintained by the MOJAVE team (Lister et al. 2009b)

REFERENCES

- Abdo A. A. et al., 2010, *ApJ*, 710, 1271
 Aharonian F. et al., 2007, *ApJ*, 664, L71
 Ajello M. et al., 2014, *ApJ*, 780, 73
 Angelakis E. et al., 2012, *Journal of Physics Conference Series*, 372, 012007
 Arshakian T. G., Ros E., Zensus J. A., 2006, *A&A*, 458, 397
 Blandford R. D., Königl A., 1979, *ApJ*, 232, 34
 Cara M., Lister M. L., 2008a, *ApJ*, 686, 148
 Cara M., Lister M. L., 2008b, *ApJ*, 674, 111
 Chatterjee R. et al., 2008, *ApJ*, 689, 79
 Cohen M. H., Lister M. L., Homan D. C., et al., 2007, *ApJ*, 658, 232
 Georganopoulos M., Kazanas D., 2004, *NAR*, 48, 403
 Ghisellini G., Padovani P., Celotti A., Maraschi L., 1993, *ApJ*, 407, 65
 Giommi P., Padovani P., Polenta G., Turriziani S., D’Elia V., Piranomonte S., 2012, *MNRAS*, 420, 2899
 Hovatta T. et al., 2014, *AJ*, 147, 143
 Hovatta T., Valtaoja E., Tornikoski M., Lähteenmäki A., 2009, *A&A*, 494, 527
 Jorstad S. G. et al., 2005, *AJ*, 130, 1418
 Komatsu E. et al., 2009, *ApJS*, 180, 330
 Lähteenmäki A., Valtaoja E., 1999, *ApJ*, 521, 493
 Lister M. L., 2001, *ApJ*, 561, 676
 Lister M. L., Aller H. D., Aller M. F., Cohen M. H., Homan D. C., et al., 2009a, *ApJ*, 137, 3718
 Lister M. L. et al., 2013, *AJ*, 146, 120
 Lister M. L. et al., 2009b, *AJ*, 138, 1874
 Lister M. L., Homan D. C., 2005, *AJ*, 130, 1389
 Lister M. L., Marscher A. P., 1997, *ApJ*, 476, 572
 Padovani P., 1992, *MNRAS*, 257, 404
 Padovani P., Urry C. M., 1992, *ApJ*, 387, 449
 Pavlidou V. et al., 2014, *MNRAS*, 442, 1693
 Pavlidou V. et al., 2012, *ApJ*, 751, 149
 Pushkarev A. B., Hovatta T., Kovalev Y. Y., Lister M. L., et al., 2012, *A&A*, 545, A113
 Pushkarev A. B., Kovalev Y. Y., Lister M. L., Savolainen T., 2009, *A&A*, 507, L33
 Readhead A. C. S., 1994, *ApJ*, 426, 51
 Urry C. M., Padovani P., 1991, *ApJ*, 371, 60
 Urry C. M., Shafer R. A., 1984, *ApJ*, 280, 569
 Vermeulen R. C., 1995, *Proceedings of the National Academy of Science*, 92, 11385
 Vermeulen R. C., Cohen M. H., 1994, *ApJ*, 430, 467